


Creation of magnetic rogue waves

Matthew G. Copus and Robert E. Camley *Center for Magnetism and Magnetic Nanostructures, University of Colorado at Colorado Springs, Colorado Springs, Colorado 80918, USA*

(Received 22 May 2020; revised 23 November 2020; accepted 25 November 2020; published 24 December 2020)

Rogue waves, first discovered in the ocean, are extraordinarily large amplitude waves which can form in relatively calm environments. Magnetic materials also support waves, but with a completely different set of underlying physics. We demonstrate the possibility of generating magnetic rogue waves by applying an abstract form of time reversal. Magnetic systems have important differences from the other media which admit rogue waves; they are inherently anisotropic and have many tunable parameters such as the magnitude and direction of an applied field. We investigate the role of anisotropy and these tunable parameters in the formation and properties of magnetic rogue waves. Through analytic calculations, we identify the important wave vectors and frequencies, typically ranging from 10 to 25 GHz, of the spin waves involved in the creation of magnetic rogue waves. We then correlate this information with the overall efficiency of the rogue wave generation process.

DOI: [10.1103/PhysRevB.102.220410](https://doi.org/10.1103/PhysRevB.102.220410)

Rogue waves in the ocean are large amplitude surface waves which far exceed the predicted height of linear wave models. The first conclusive evidence of the existence of rogue waves was obtained in 1995 when an exceptionally tall ocean wave struck the Draupner platform in the North Sea [1]. Since then, there have been experiments to reproduce and study water rogue waves under controlled conditions in a laboratory. These experiments employed different methods of generating rogue waves, including the application of time reversal [2,3] and the manipulation of the intersection angle of two interfering waves [4]. Rogue waves have also been observed in other contexts, including second sound waves in superfluid helium [5] and pulses of broadband light in nonlinear optics [6] and in microwave cavities in the linear regime [7]. The original view of an ocean rogue wave was of a relatively high amplitude wave which arises unexpectedly from random wave configurations. However, for this paper, we adopt a more general definition of a rogue wave as being any wave localized in time and space and with an amplitude which is drastically larger than the surrounding population of waves.

Here we search for rogue waves in magnetic systems. Magnetic materials are significantly different from many other systems in that they are naturally anisotropic, and they have tunable parameters that determine wave properties. Magnetic rogue waves (MRWs) have a variety of potential applications. Through the process presented in this paper, we have found that MRWs can be generated at virtually any location on a thin magnetic material. We have also found that the amplitude of a generated MRW can be controlled to a large extent. Their addressability and the capacity to control their intensity may make MRWs suitable for performing spin wave logic and for applications in spintronic devices [8–11]. In addition, MRWs with complex geometries can be constructed, which may give them use in encryption and secure communications [12].

We note that these rogue waves are not solitons, which have been extensively explored in magnetic systems [13–17]. In

fact, the creation of rogue waves requires that they decay as a function of time, as will be seen below.

To generate MRWs we use a time reversal process consisting of two phases: recording and reemission. The recording phase begins with the spins in plane in an equilibrium state. A small region of spins is then brought up to 2° out of plane to establish an initial MRW [Fig. 1(a)]. The MRW is then allowed to decay, creating spin waves which radiate anisotropically [Fig. 1(b)] and reflect several times off the material's boundaries before dissipating due to damping [Fig. 1(c)]. An array of sensors, located throughout the material, records the out-of-plane magnetic field in the material during the decay process. The reemission phase again begins in equilibrium. Each sensor in the array reemits the time reversed magnetic field data which they each uniquely recorded [Fig. 1(d)]. To compensate for losses in amplitude during the wave's movement between the MRW source and a given sensor, the data is reemitted at an intensity several times the recorded value. These reemitted waves interfere [Fig. 1(e)] in such a way to reconstruct the MRW at its original location while simultaneously producing a nearzero amplitude in the remainder of the material [Fig. 1(f)]. Videos of the recording and reemission phases for Fig. 1 are available in the Supplemental Material [18].

It is not immediately obvious that the process described above will produce MRWs, for several reasons. First, it is not a true time reversal. Only the out-of-plane fields are recorded and replayed. The fields within the plane of the film are neglected. Second, the spins in the region of the replayed dynamic fields do not precess backwards. Third, as noted above, damping is important in breaking time reversal in both the recording and reemission phases.

The numerical simulations for Fig. 1 were carried out with the micromagnetic program MUMAX³. In general, we use a cell size of $5 \times 5 \times 5 \text{ nm}^3$ with a mesh of $128 \times 128 \times 1$ cells. An external field of $\mu_0 H_0 = 0.1 \text{ T}$ is applied in plane. The

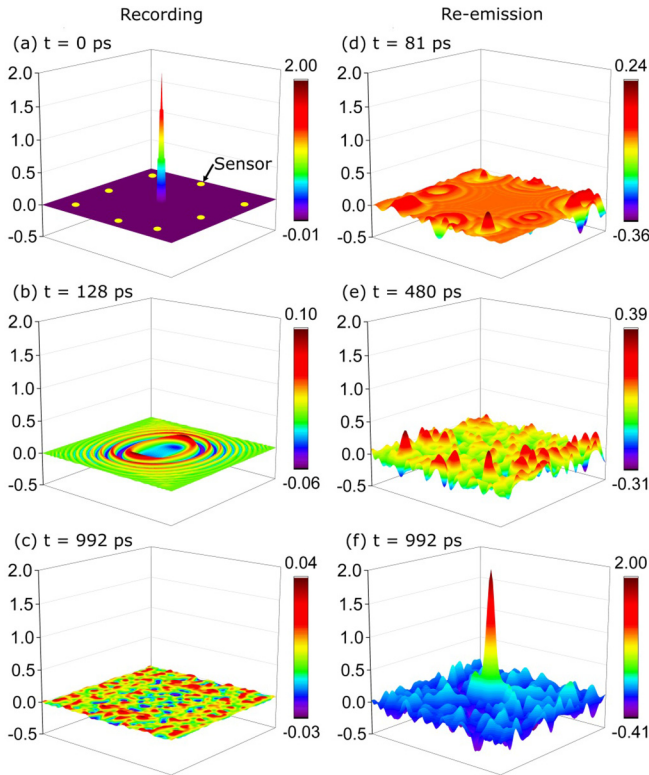


FIG. 1. Out-of-plane angle measurements (degrees) during the recording and reemission phases of a simulated magnetic rogue wave reconstructed through time reversal. (a) Initial rogue wave whose decay is recorded by sensors positioned throughout the material. (b) Anisotropic decay of the initial rogue wave. (c) End of the recording phase after significant damping. (d) Reemission of sensor data. (e) Constructive and destructive interference. (f) Reconstruction of the magnetic rogue wave at the end of the reemission phase.

simulated material is a Permalloy with a saturation magnetization of $M_s = 800$ kA/m and magnetic damping parameter of $\alpha = 0.006$. The time-step size is 0.05 ps and the simulation has a total duration of 1 ns (20 000 steps). The out-of-plane magnetic field strength is recorded at the sensor sites at each time step and is averaged over the sensor area. Each sensor has a square geometry and covers an area of 625 nm². The reemitted data are multiplied by a factor of 17. We use an array of eight sensors which surrounds the MRW source, as can be seen in Fig. 1(a). The initial MRW has a diameter of 25 nm (5×5 cells) at its base and is excited 2° out of plane at its peak. The cross section of the initial MRW is shaped like a Gaussian curve.

Like Przadka *et al.* we define the quality of reconstruction as a peak-to-noise ratio (PNR) as the ratio between the peak intensity of the MRW and the mean side-lobe intensity at the time of reconstruction [2]. Both the peak and noise intensities are measured in degrees out of plane. We define the time of reconstruction as the time step at which the reconstructed wave reaches its maximum amplitude during the reemission phase. The exact time of reconstruction can vary slightly based on a variety of system parameters but usually occurs within 10 ps of the duration of the recording phase.

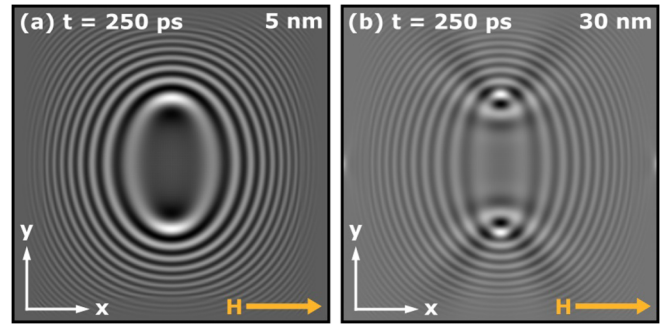


FIG. 2. Anisotropic decay of a magnetic rogue wave calculated for Permalloy films with thicknesses of (a) 5 nm and (b) 30 nm. For both thicknesses, an external field, H , is applied in plane along the x axis.

We have investigated how the reconstruction of MRWs in our standard system depends on the variation of several system parameters. We summarize a number of our findings as follows:

(1) Even one sensor can produce a distinct reconstructed peak with a PNR near 10, provided there are several reflections during the recording phase. Increasing the number of sensors to twelve produces a PNR around 29.

(2) The root mean square of the field strength recorded by a sensor is around 0.17 mT, with a maximum amplitude of around 1.1 mT. These values are primarily affected by sensor position, magnetic damping, and the height of the initial MRW.

(3) The PNR increases with the duration of the recording phase until the time where damping significantly reduces the overall amplitude of the waves. After such time, any recorded information no longer has a relevant impact on the reconstruction process. For $\alpha = 0.006$ this point occurs at around 1.5 ns.

(4) Multiple MRWs can be generated simultaneously. For example, by using eight sensors, we have created up to ten MRWs positioned randomly throughout the material.

(5) The PNR decreases exponentially with increasing α . Increased damping results in a reduction in the amount of information collected by the sensors over time, causing the lower PNR values.

(6) The PNR depends on both the initial amplitude of the MRW and the multiplication factor. In general, the PNR increases as a function of either parameter, but saturates at a value of approximately 24. The saturation occurs near a value of 6 for the multiplication factor and at an angle of about 2° for the initial MRW.

As mentioned previously, magnetic systems involve the issues of anisotropy and tunability. This can be demonstrated in several ways. For example, the thickness of the material has a significant impact on the anisotropic nature of how spin waves propagate, as can be seen in Fig. 2. Figures 2(a) and 2(b) show the anisotropic decay of an MRW in films with thicknesses of 5 and 30 nm, respectively. Figures 2(a) and 2(b) both result from an MRW raised 2° out of plane at the center of the material. This MRW was allowed to decay for a period of 1 ns with an external field of $\mu_0 H_0 = 0.1$ T oriented in plane, along the x axis. Figure 2 shows that the concentric waves in the 30 nm film have greater eccentricity than concentric

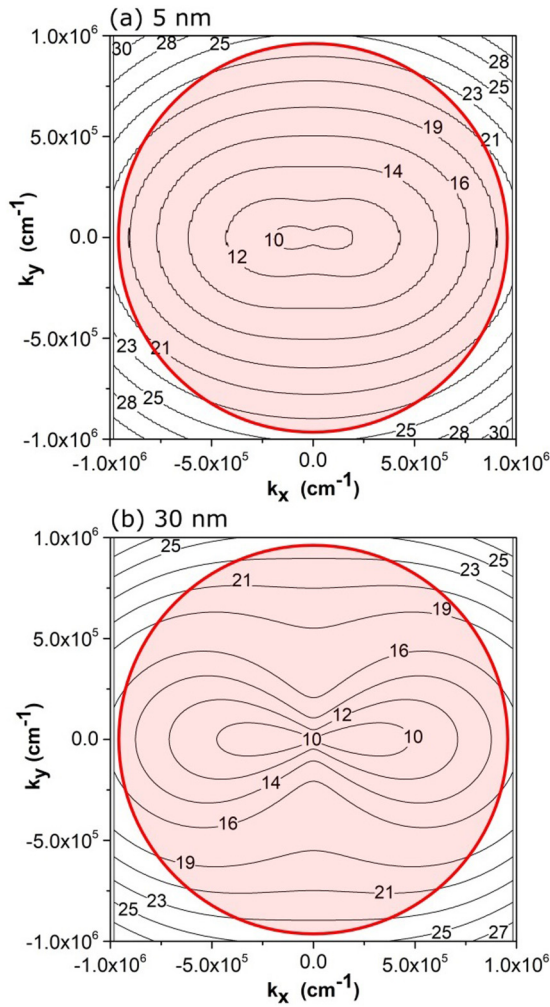


FIG. 3. Analytic calculations of the isofrequency curves for a (a) 5 nm film and a (b) 30 nm film. The red shaded area indicates the typical wave vectors involved in the decay of a magnetic rogue wave. Strong self-focusing and caustics occur in directions perpendicular to where the isofrequency curves have near zero curvature.

waves in the 5 nm film. Also, the 30 nm film shows beaming occurring near the top and bottom of the central ellipse at approximately 45° angles with respect to the external field direction.

To understand this anisotropic behavior and its effect on the creation of MRWs, we analyzed the frequencies produced during the recording phase. We performed a Fourier transform on the initial rogue wave configuration to determine the relevant wave vectors. We indicate the most important wave vectors by the shaded circles in Fig. 3, which also shows the calculated [19] isofrequency curves for the 5 and 30 nm films with $\mu_0 H_0 = 0.1$ T. What is particularly important is that regions where the curvature is near zero, i.e., flat regions, on the iso-frequency curves can lead to strong self-focusing and caustics [20–22] in directions perpendicular to the isofrequency curves. This gives rise to significant differences in the intensity of spin waves propagating in different directions. One result of this focusing, for both thicknesses, is that the largest amplitude spin waves will occur perpendicular to the external field direction.

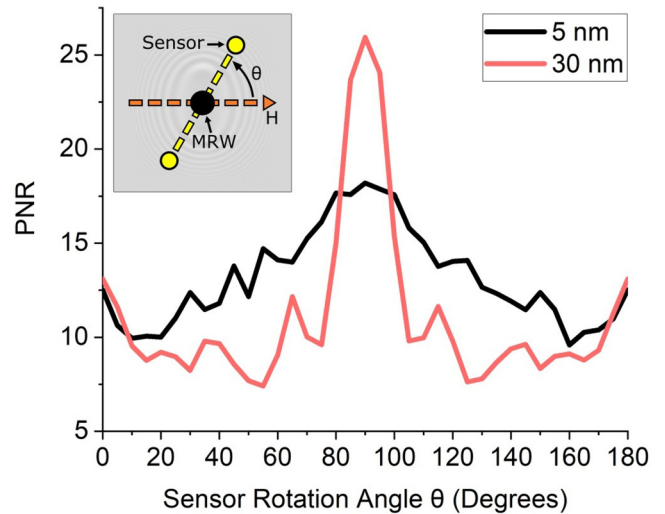


FIG. 4. Peak-to-noise ratio (PNR) as a function of the angle, θ , between the direction of the external field, H , and a line drawn between two sensors positioned equidistant from a magnetic rogue wave (MRW) source calculated for Permalloy films with thicknesses of 5 and 30 nm.

The initial decomposition of the rogue wave involves multiple issues: multiple spin waves with different wavevectors are generated, each propagating with different group velocities [23]. At low wave vectors, magnetostatic effects are important, while larger wave vector modes are dominated by exchange interactions. In addition, nonlinearity may play a role. All these effects are automatically included in the micromagnetic calculations.

For some portions of the recording and reconstruction, nonlinear effects could be important. We have checked whether the linear results in Fig. 3 are still appropriate in the nonlinear limit through the micromagnetic modeling. Indeed, even for large amplitude oscillations, the micromagnetic results are nearly equivalent to the linear results shown in Fig. 3 except that higher order harmonic frequencies are also generated.

We conducted a series of simulations which explored how sensor placement with respect to the external field direction affects MRW reconstruction. Two sensors were positioned equidistant from and on opposite sides of an initial MRW source at the center of the material. These sensors were then rotated counterclockwise around the MRW source in 5° increments. At each increment, a simulation was performed to determine the system’s PNR. The decision to keep the sensors a fixed distance from the MRW source was intended to avoid variations in the recorded field intensities based on the proximity of the sensors to the source. The results of this series of simulations are shown in Fig. 4. PNR varies significantly with the sensor rotation angle, θ , with a substantially larger variation present for the 30 nm film. The maximums for both thicknesses occur when θ is at 90°, which corresponds to the primary direction for the self-focusing discussed above.

We have already shown how the orientation of the external field with respect to the sensors can affect the reconstruction of an MRW. Another parameter is the strength of the external field. Figure 5 shows how the peak and noise signals depend

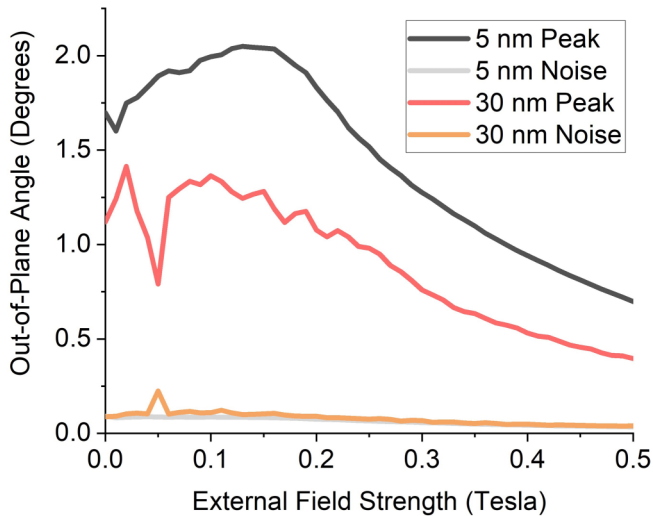


FIG. 5. Peak and noise amplitudes measured in degrees out of plane as functions of external field strength for a reconstructed magnetic rogue wave calculated for Permalloy films with thicknesses of 5 and 30 nm.

on the magnitude of the external field. For both thicknesses, the peak height remains nearly constant for low fields and then steadily decreases as the external field increases. We believe this is ultimately caused by the damping in the material. If one looks at the Landau-Lifshitz-Gilbert equation, one sees the damping term depends on a term that is given by $\alpha d\mathbf{M}/dt$. For an excitation of frequency ω , the damping becomes proportional to $\alpha\omega$. Increasing the external field pushes the spin wave band to higher frequencies, increasing the effective damping, resulting in a smaller reconstructed peak.

It is of interest to know how robust this time reversal process is for creating MRWs, i.e., does it only work in an ideal system? We performed several simulations that explored how rough boundaries and holes in the film would affect the PNR of a reconstructed MRW. With nearly all forms of imperfection that we simulated, we saw some decrease in the PNR, but the reconstruction still remained quite good. Videos of the recording and reemission phases of a system with rough boundaries and a system with holes are available in the Supplemental Material [18].

We comment on the possibility of experimental observation of these rogue waves. First, the dynamic fields used in our simulations are relatively large, on the order of 3 mT. We note that fields this large are possible in a coplanar waveguide [24] and fields an order of magnitude larger have already been produced in microstrip configurations with small cross-sectional areas [25]. Furthermore, if the experiment was performed on a material with low α such as yttrium-iron garnet (YIG) [26] or

cobalt-iron heterostructures [27], the required dynamic fields would be smaller than the ones used here. Second, our rogue wave has a spatial extent of roughly 30 nm and a time response of under one nanosecond. Resolutions of 30 nm are possible in magnetic force microscopy (MFM) systems [28]; however, the time resolution is a problem. Typical MFM measurements have timescales of around 100 ms, too slow to measure the nanosecond time scale required here. However, laser probes can measure in the femtosecond scale, albeit often with larger diameter beams. Recently there have been reports of magneto-optical microscopy with a spatial resolution of under 200 nm and picosecond time resolution [29]. This should be sufficient to see the rogue waves.

For the recording process, it is difficult to measure the dynamic fields directly on such a small scale. However, it is not necessary. One can use micromagnetic simulations to calculate the required fields to produce any particular rogue wave. Additionally, it is possible to measure the magnetization motion on very small spatial scales and at picosecond time resolution [30,31]. In some cases, one can use the Landau-Lifshitz-Gilbert equations, with a known $\mathbf{M}(t)$, to calculate the required dipole fields at a sensor site.

Our calculations show that MRWs with diameters as large as $1 \mu\text{m}$ can be reconstructed in a $12.8 \mu\text{m} \times 12.8 \mu\text{m} \times 30 \text{ nm}$ YIG film using $1 \mu\text{m}$ diameter sensors. YIG's relatively low α and M_s allow for large spin wave propagation lengths with minimal anisotropic behavior, leading to well-defined reconstruction. This should allow for easier experimental verification, for example by scanning tunneling microscopy [32].

In summary, magnetic rogue waves can be created in thin magnetic films. The efficiency of MRW generation depends on the parameters of the material they are created in, the external field strength and direction, the initial MRW amplitude and shape, the number of sensors and their placement, and the reemission multiplication factor. Multiple MRWs and MRWs with complex shapes can be reconstructed. In this paper we have concentrated on producing rogue waves near the linear, small amplitude regime where nonlinear effects only play a small role. It will be interesting to extend this further into the nonlinear regime and observe the differences. Additionally, unlike in water where waves propagate through the short-range interaction of neighboring water molecules, magnetic waves propagate through both short-range (exchange) and long-range (dipolar) effects. It is worth considering how both effects contribute the formation of MRWs. Our preliminary simulations on this matter show that it is possible to generate an MRW purely through dipolar interaction.

The authors thank Pavel Kabos and Dmytro Bozhko for helpful discussions.

- [1] C. Kharif, E. Pelinovsky, and A. Slunyaev, *Rogue Waves in the Ocean*, Advances in Geophysical and Environmental Mechanics and Mathematics (Springer, Berlin, 2008).
 [2] A. Prasadka, S. Feat, P. Petitjeans, V. Pagneux, A. Maurel, and M. Fink, *Phys. Rev. Lett.* **109**, 064501 (2012).

- [3] A. Chabchoub and M. Fink, *Phys. Rev. Lett.* **112**, 124101 (2014).
 [4] M. L. McAllister, S. Draycott, T. A. A. Adcock, P. H. Taylor, and T. S. van den Bremer, *J. Fluid Mech.* **860**, 767 (2019).

- [5] V. B. Efimov, A. N. Ganshin, G. V. Kolmakov, P. V. E. McClintock, and L. P. Mezhov-Deglin, *Eur. Phys. J.: Spec. Top.* **185**, 181 (2010).
- [6] D. R. Solli, C. Ropers, P. Koonath, and B. Jalali, *Nature (London)* **450**, 1054 (2007).
- [7] R. Höhmann, U. Kuhl, H.-J. Stöckmann, L. Kaplan, and E. J. Heller, *Phys. Rev. Lett.* **104**, 093901 (2010).
- [8] S. A. Wolf, A. Y. Chtchelkanova, and D. M. Treger, *IBM J. Res. Dev.* **50**, 101 (2006).
- [9] S. A. Wolf, D. D. Awschalom, R. A. Buhrman, J. M. Daughton, S. von Molnár, M. L. Roukes, A. Y. Chtchelkanova, and D. M. Treger, *Science* **294**, 1488 (2001).
- [10] B. Behin-Aein, D. Datta, S. Salahuddin, and S. Datta, *Nat. Nanotechnol.* **5**, 266 (2010).
- [11] F. Heussner, A. A. Serga, T. Brächer, B. Hillebrands, and P. Pirro, *Appl. Phys. Lett.* **111**, 122401 (2017).
- [12] S. Ghosh, *Proc. IEEE* **104**, 1864 (2016).
- [13] V. Bar'yakhtar, M. Chetkin, B. Ivanov, and S. Gadetskii, *Dynamics of Topological Magnetic Solitons: Experiment and Theory*, Springer Tracts in Modern Physics (Springer, Berlin, 2006).
- [14] A. Kosevich, B. Ivanov, and A. Kovalev, *Phys. Rep.* **194**, 117 (1990).
- [15] S. Bonetti, R. Kukreja, Z. Chen, F. Macià, J. M. Hernández, A. Eklund, D. Backes, J. Frisch, J. Katine, G. Malm, S. Urazhdin, A. D. Kent, J. Stöhr, H. Ohldag, and H. A. Dürr, *Nat. Commun.* **6**, 8889 (2015).
- [16] K. Maki and P. Kumar, *Phys. Rev. B* **14**, 118 (1976).
- [17] K. S. Buchanan, P. E. Roy, M. Grimsditch, F. Y. Fradin, K. Y. Guslienko, S. D. Bader, and V. Novosad, *Nat. Phys.* **1**, 172 (2005).
- [18] See Supplemental Material at <http://link.aps.org/supplemental/10.1103/PhysRevB.102.220410> for videos of the recording and remission phases for the reconstruction of a magnetic rogue wave using eight sensors, including results in a material with rough boundaries and in a material with holes.
- [19] T. Wolfram and R. DeWames, *Prog. Surf. Sci.* **2**, 233 (1972).
- [20] V. Veerakumar and R. E. Camley, *Phys. Rev. B* **74**, 214401 (2006).
- [21] T. Schneider, A. A. Serga, A. V. Chumak, C. W. Sandweg, S. Trudel, S. Wolff, M. P. Kostylev, V. S. Tiberkevich, A. N. Slavin, and B. Hillebrands, *Phys. Rev. Lett.* **104**, 197203 (2010).
- [22] J.-V. Kim, R. L. Stamps, and R. E. Camley, *Phys. Rev. Lett.* **117**, 197204 (2016).
- [23] A. Kamimaki, S. Iihama, Y. Sasaki, Y. Ando, and S. Mizukami, *Phys. Rev. B* **96**, 014438 (2017).
- [24] Y. S. Gui, A. Wirthmann, and C.-M. Hu, *Phys. Rev. B* **80**, 184422 (2009).
- [25] Y. Khivintsev, J. Marsh, V. Zagorodnii, I. Harward, J. Lovejoy, P. Krivosik, R. E. Camley, and Z. Celinski, *Appl. Phys. Lett.* **98**, 042505 (2011).
- [26] C. Hauser, T. Richter, N. Homonnay, C. Eisenschmidt, M. Qaid, H. Deniz, D. Hesse, M. Sawicki, S. G. Ebbinghaus, and G. Schmidt, *Sci. Rep.* **6**, 20827 (2016).
- [27] L. Flacke, L. Liensberger, M. Althammer, H. Huebl, S. Geprägs, K. Schultheiss, A. Buzdakov, T. Hula, H. Schultheiss, E. R. J. Edwards, H. T. Nembach, J. M. Shaw, R. Gross, and M. Weiler, *Appl. Phys. Lett.* **115**, 122402 (2019).
- [28] L. Abelmann, S. Porthun, M. Haast, C. Lodder, A. Moser, M. E. Best, P. J. van Schendel, B. Stiefel, H. J. Hug, G. P. Heydon, A. Farley, S. R. Hoon, T. Pfaffelhuber, R. Proksch, and K. Babcock, *J. Magn. Magn. Mater.* **190**, 135 (1998).
- [29] N. O. Urs, B. Mozooni, P. Mazalski, M. Kustov, P. Hayes, S. Deldar, E. Quandt, and J. McCord, *AIP Adv.* **6**, 055605 (2016).
- [30] J. Förster, S. Wintz, J. Bailey, S. Finizio, E. Josten, C. Dubs, D. A. Bozhko, H. Stoll, G. Dieterle, N. Träger, J. Raabe, A. N. Slavin, M. Weigand, J. Gräfe, and G. Schütz, *J. Appl. Phys.* **126**, 173909 (2019).
- [31] J. W. Lau and J. M. Shaw, *J. Phys. D* **44**, 303001 (2011).
- [32] S. Yan, L. Malavolti, J. A. J. Burgess, A. Droghetti, A. Rubio, and S. Loth, *Sci. Adv.* **3**, e1603137 (2017).